



UiO-66-NH₂: a recyclable and efficient sorbent for dispersive solid-phase extraction of fluorinated aromatic carboxylic acids from aqueous matrices

Anuj Kumar¹ · Chhaya Sharma¹

Received: 20 March 2023 / Revised: 15 April 2023 / Accepted: 2 May 2023 / Published online: 17 May 2023
© Springer-Verlag GmbH Germany, part of Springer Nature 2023

Abstract

The present study describes the trace analysis of 23 fluorinated aromatic carboxylic acids based on the dispersive solid-phase extraction (dSPE) technique using UiO-66-NH₂ MOF as efficient, recyclable sorbent, and GC–MS negative ionization mass spectrometry (NICI MS) as determination technique. All 23 fluorobenzoic acids (FBAs) were enriched, separated, and eluted in a shorter retention time; the derivatization was done by pentafluorobenzyl bromide (1% in acetone), in which the use of inorganic base K₂CO₃ was improved by triethylamine to increase the lifespan of the GC column. The performance of UiO-66-NH₂ was evaluated by dSPE in Milli-Q water, artificial seawater, and tap water samples, and the impact of various parameters on the extraction efficiency was investigated by GC–NICI MS. The method was found to be precise, reproducible, and applicable to the seawater samples. In the linearity range, the regression value was found to be >0.98; LOD and LOQ were found to be in the range of 0.33–1.17 ng/mL and 1.23–3.33 ng/mL, respectively; and the value of the extraction efficiency was found to range between 98.45 and 104.39% for Milli-Q water samples, 69.13–105.48% for salt-rich seawater samples, and 92.56–103.50% for tap water samples with a maximum RSD value of 6.87% that confirms the applicability of the method to different water matrices.

Keywords UiO-66-NH₂ · Dispersive solid-phase extraction · GC–MS · Negative ion chemical ionization · Fluorobenzoic acids · Pentafluorobenzyl bromide

Introduction

The development in the sample pretreatment techniques like SPE has become very popular nowadays for the fast and inexpensive analysis. dSPE is one of the advanced and efficient extraction techniques with significant advantages over traditional SPE technique due to its simplicity, rapid analysis, and more contact area of sorbent with the analyte as it is not in the case of SPE cartridge [1]. Different sorbent materials [2, 3] have been developed for this type of extraction; however, metal–organic frameworks (MOFs) have been reported as efficient sorbents in many applications due to their high surface

area, tunable porosity, high crystallinity, and good thermal stability. MOFs have great potential for various applications, such as gas storage [4–9], catalysis [10], drug delivery [11], biomedicine, and electrochemistry [12–14], and are also studied as sorbents for removing contaminants from water, air, or fuel. UiO-66 amino derivative MOF shows excellent stability in the water matrix [15], due to which it holds potential for various water-based applications [16–18].

Fluorobenzoic acids are very important chemical tracers in the enhanced oil recovery process due to their non-toxicity over radioactive tracers [19] and lower detection levels. Hence, their detection at the lowest concentration is the main objective of the chemists to reduce the cost of the enhanced oil recovery (EOR) process since lower LOD causes a reduction in the amount of FBAs to be injected into the injector well. Kumar et al. [20] compiled all the methods and techniques for determining FBAs in the aqueous medium, and the GC-based methods were found suitable for achieving a very low detection limit

✉ Chhaya Sharma
chhaya.sharma@pt.iitr.ac.in

¹ GC-MS Laboratory, Department of Paper Technology, Indian Institute of Technology Roorkee, Uttar Pradesh, Saharanpur Campus, Saharanpur 247001, India

after derivatization. Negative ion chemical ionization (NICI) was chosen in this study to analyze FBAs since it is specific for halogens, and a lower detection limit can be achieved with this ionization mode. Another advantage of the NICI mode is the less reaction time required for the derivatization of FBAs to their pentafluorobenzyl esters [21]. However, a strong base was required for the reaction to occur. Galdiga et al. [21] used inorganic base solid potassium carbonate (K_2CO_3) for the derivatization purpose, but it reduced the performance of the GC column due to its accumulation on the column head as it is non-volatile, so periodic trimming of the GC column was required to recover the performance. As a result, the column's capacity factor changed after every trim, and the length of the column also gradually decreased after introducing every five injections. To overcome this disadvantage, organic base triethylamine was employed, and the reaction yield was found to be similar to the K_2CO_3 only by adding 50 μ l volume of it.

Several reported methods [21–27] described the SPE-based method for extraction of FBAs from water samples. However, these methods required large sample volume, solvent volume, and various steps before sample loading for extraction. Further, SPE cartridges are generally single-use, so a recyclable material UiO-66- NH_2 MOF was synthesized, characterized, and applied as sorbent material for the dSPE of the 23 different isomers of FBAs. The synthesized material exhibited better adsorption for FBAs owing to the mechanism of interaction, i.e., hydrogen bonding between the amino functional group and fluorine atom of FBAs, and the interaction between Zr atom and oxygen of carbonyl of FBAs. In terms of better sensitivity, the negative ion chemical ionization technique was used in MS, and all the 23 FBAs were derivatized using pentafluorobenzyl bromide (1% in acetone), similar to Galdiga et al. [21] with the replacement of inorganic base K_2CO_3 by triethylamine and separated on a GC column having 5% phenyl 95% polysilphenylene siloxane as stationary phase. Since produced water contains various dissolved organics, inorganics, and gases [28–31], inorganic salts are the primary component of it. Therefore, an artificial seawater sample was prepared as a representative sample to evaluate the method's performance.

The method describes the rapid, precise, easiest, and validated method for analysis of 23 FBAs at in Milli-Q, artificial seawater matrix, and tap water matrix along with the reduced LOD level (up to 0.33 ng/mL) as compared to other GC-based methods. The specific advantage is also offered by MOF, which can be reused for up to three cycles and may replace the traditional SPE sorbent materials, which are disposable in most cases.

Experimental

Chemicals and reagents

All 23 FBAs were purchased from Sigma-Aldrich. Zirconium chloride and BDC- NH_2 (2-amino terephthalic acid) were also procured from Sigma-Aldrich. The derivatizing reagent PFBBr (99%) was purchased from Sigma-Aldrich. All solvents, including acetonitrile and methanol, were of gradient grade, and ultra-pure water was produced from the Milli-Q water purification system (Millipore-Merck, USA). The reagents, including dimethyl formamide (DMF), triethylamine, and HCOOH (85%), were of analytical grade. The details of each FBA are defined in Table S1 (see Electronic Supplementary Material Table S1).

Instrumental details

GC–MS apparatus and conditions

Trace GC Ultra with DSQ (Thermo Finnigan Pvt. Ltd., USA) equipped with liquid autoinjector AI/AS 3000 was used as a determination technique. TR-05 column (60 m \times 0.25 mm \times 0.25 μ m film thickness) was used for separating the pentafluorobenzyl (PFB) derivatives of FBAs by temperature gradient program with the carrier gas (Helium) flow rate of 1 mL/min. The temperature program was initial temperature 60°C and held for 1 min, then increased to 175°C at the rate of 5.5°C/min and held for 5 min, and then finally to 250°C with a heating rate of 3°C/min and hold time of 3 min. The total run time was 32 min, and the temperature of the ion source, inlet, and MS transfer line was 230°C, 250°C, and 280°C, respectively. The other parameters were ion source, negative ion chemical ionization; reagent gas, methane; the flow rate of reagent gas, 2.2 mL/min; ion source temperature, 135°C; injection, splitless; splitless time, 0.5 min; and injector temperature, 250°C. The analysis was done using SIM ions with a SIM width of 1.0.

Powdered X-ray diffraction

The crystallinity and stability of the synthesized MOF were determined using the PXRD technique (Rigaku Ultima IV, Japan). The XRD pattern was recorded in the angle range (2θ) of 5–80° at the scan rate of 5°/min using Cu $K\alpha$ radiation ($\lambda = 0.15405$ nm).

Fourier transform infrared spectroscopy (FTIR)

The FTIR technique was used to investigate the functional groups present in the synthesized MOF and the change in

their intensity/wavenumber after interaction with FBAs by making KBr pellets of the samples under 10.0-ton hydraulic pressure. The USA model, FTIR spectrum 2 of Perkin Elmer, was utilized to execute the FTIR scans with a wavenumber bracket of 4000–600 cm⁻¹. For every sample, 32 scans were performed with a resolution of 4 cm⁻¹.

Morphology and elemental analysis

In the morphological study of MOF, changes in the morphology of the synthesized MOF after interaction with FBAs were investigated using field emission scanning electron microscope (FESEM) MIRA3 FESEM TESCAN, USA. The elemental analysis was done using EDAX in both cases.

Surface area and pore size measurement

The pore size determination and surface area analysis of the synthesized MOF was done by a surface area analyzer (Autosorb IQ, USA) based on Brunauer–Emmett–Teller (BET) theory. The degassing of the MOF was done at 120°C for 8 h prior to the surface area measurement.

X-ray photoelectron spectroscopy (XPS)

The XPS spectra of UiO-66-NH₂ and UiO-66-NH₂ + 2-TFM were recorded to understand the various bonds in the MOF. The XPS was performed by an X-ray photoelectron spectrometer (PHI-5000 Versa Probe III, ULVAC-PHI Inc., USA), employing Al K α as a radiation source. The analyzer pass energies were 280 eV for survey scan and 55 eV for individual elements. The C1s peak at 284.6 eV was taken as the reference for calibrating binding energy.

Synthesis of UiO-66-NH₂

UiO-66-NH₂ was prepared according to the previously reported methods [32], with some minor modifications. In a typical solvothermal synthesis of UiO-66-NH₂, 7.6 g ZrCl₄ and 4.34 g 2-amino terephthalic acid were mixed with 72 mL DMF and stirred for 2.0 h for proper mixing. The crystallization was done in a Teflon autoclave reactor at 150°C for 24 h. The resultant solid was filtered and washed with DMF three times to remove the residuals of the unreacted part. The resultant solid was transferred to a conical flask, and the solvent exchange reaction was carried out using dichloromethane, as a higher surface area was reported using this solvent [33]. This reaction was repeated five times, and then the solid was dried at 100°C for 8 h and stored at room temperature.

Sample preparation

The individual stock of each FBA was prepared in acetonitrile and spiked the appropriate volume of it in the Milli-Q water/seawater sample to get the final concentration at ng/mL level. The solution was stirred for 5 min to make the solution homogenized.

Dispersive SPE and derivatization procedure

The dispersive SPE was carried out according to the following steps: (1) 20 ml of the Milli-Q water containing 1 ng/mL of FBAs was put into a 50 ml Beaker; (2) 80 mg of UiO-66-NH₂ sorbent material was added to this solution and stirred for 5 min and sonicated for 10 min to disperse the MOF particles in the aqueous solution and to promote the transfer of FBAs to the MOF particles; and (3) the mixture was centrifuged for 10 min at 6440 \times g, the supernatant aqueous solution was discarded, and the mixture was dried under a nitrogen stream. FBAs were eluted by adding 3.0 ml of ACN containing 5% HCOOH by ultrasonication of 7 min. (4) This mixture was dried under a nitrogen stream, and the residue was dissolved in 700 μ L of ACN and filtered through a 0.22- μ m nylon filter already conditioned with ACN. Then this solution was transferred to a 2.0 ml reaction vial and proceeded for derivatization.

The derivatization procedure was performed as follows:

Add 200 μ L PFBBr solution (1% in acetone) and 50 μ L of triethylamine into 700 μ L ACN containing FBAs, and mix this solution using a vortex mixer for 5 min. This solution was put at 95°C for 30 min in preheated oven. After the reaction got completed, the vial was cooled to attain room temperature, and 1 μ L of this solution was injected splitless into the GC–MS to get the response of the FBA PFB esters.

Improvement in the derivatization step

The derivatization procedure was already reported by Galdiga et al. [21], in which the use of pentafluorobenzyl bromide (1% in acetone) with inorganic base K₂CO₃ was described. In this study, the use of K₂CO₃ was improved by triethylamine, and the concentration and volume of the pentafluorobenzyl bromide (PFBBr) were also reduced to remove the interfering background of it as described by Kumar et al. [34]. Since inorganic bases are non-volatile in nature and they may get deposited permanently on the column head or injector port, which reduces the performance of the column as well as the volume of the sample to be injected, due to which a periodic trimming is required to recover the performance of the column, the use of triethylamine was found the suitable base for this reaction.

Results and discussion

Separation of FBAs on GC column

In this study, 23 FBAs as their pentafluorobenzyl esters (PFB esters) were well separated on 5% phenyl polysilphenylene siloxane based 60 m × 0.25 mm ID × 0.25 μm film thickness (TR-05 MS) GC column at their [M-1] SIM ions. The mutual resolution between the different FBAs was found to be very good (see Electronic Supplementary Material Fig. S2).

Characterization of the sorbent

The synthesized MOF was characterized by XRD, BET, FESEM, FTIR, and EDX. The XRD pattern (Fig. 1b.) of the synthesized UiO-66-NH₂ in which the characteristic peaks at 7.37°, 8.48°, and 25.70° corresponding to (1,1,1), (2,0,0), and (6,0,0) diffraction planes, respectively, confirmed the successful preparation of this MOF [35]. The synthesized MOF was also analyzed by a BET surface area analyzer that showed the BET surface area of 308.66 m²/g and Langmuir surface area of 414 m²/g, pore size of 12.47 Å. Figure 2a shows the morphology of the MOF particles that were obtained using FESEM, in which the MOF particles were found nearly spherical in shape and aggregated into larger particles. The FTIR spectra (Fig. 1a) were recorded using KBr pellets in which the characteristic peaks at 1570 cm⁻¹, 1651 cm⁻¹, 1485 cm⁻¹, 1385 cm⁻¹, 1254 cm⁻¹, 1020 cm⁻¹, and 768 cm⁻¹ was observed corresponding to the reaction

between Zr⁴⁺ and COOH of BDC-NH₂, C-O asymmetric stretching, C=C aromatic bond [33], symmetric stretching of C-O bond, aromatic C-N bond, Zr-OH bending vibration [36], and Zr-O stretching vibration, respectively [35], and the characteristic band at 3340 cm⁻¹ corresponds to the amino group. Thus, the FTIR spectra confirm the successful preparation of UiO-66-NH₂.

In order to evaluate the interaction between UiO-66-NH₂ and FBAs, the FTIR spectra of UiO-66-NH₂ were also recorded after interaction with FBA in which the peak at 1155 cm⁻¹ corresponding to C-F bond appeared, and the intensity of the peak at 1250 cm⁻¹ (C-O stretching frequency) was changed due to shifting the electron cloud of the carbonyl group to Zr atom corresponding to the interaction between the carbonyl of the FBAs and Zr of MOF, which was further confirmed by the increased intensity of Zr-O bond. On the other hand, the peak broadening and increased intensity of the amino peak at 3340 cm⁻¹ was also observed due to possible hydrogen bonding between the amino group of UiO-66-NH₂ and fluorine of the FBAs, so the amino moiety was also the interaction site for the FBAs [37]. Another observation was found at the peak 1651 cm⁻¹, which corresponds to the COOH group of BDC-NH₂, but after the interaction, one more peak at 1674 cm⁻¹ was observed, possibly corresponding to the COOH group of the FBAs, which also confirms the successful interaction of the FBAs with UiO-66-NH₂.

The energy dispersive X-ray analysis (EDAX) pattern was also recorded at the interaction site of UiO-66-NH₂

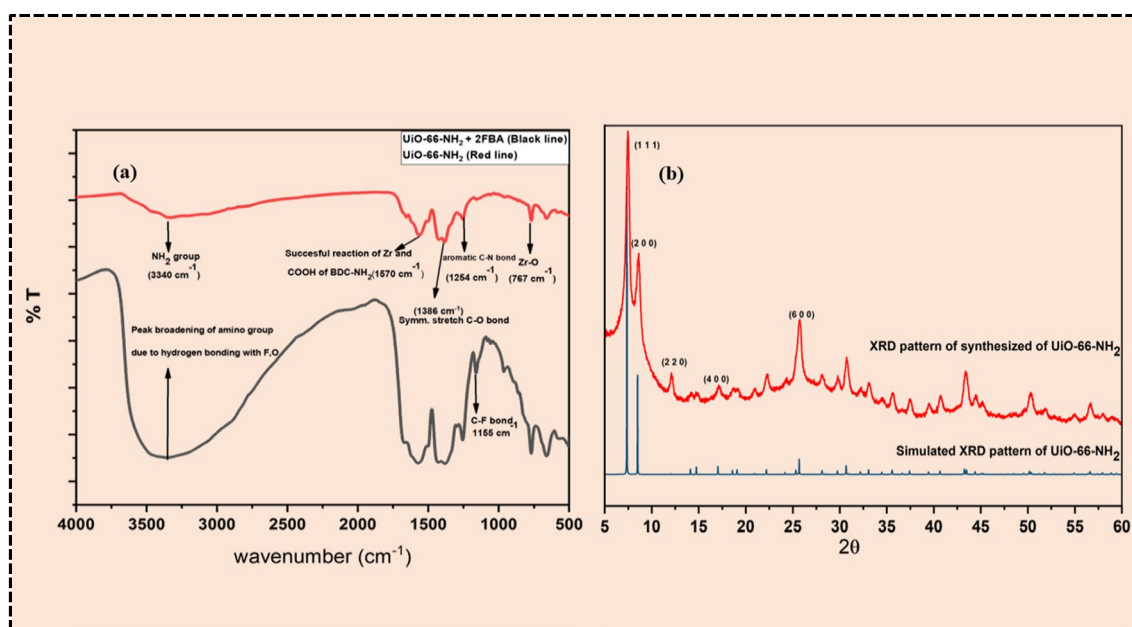


Fig. 1 a FTIR spectra of UiO-66-NH₂ and UiO-66-NH₂ + 2-FBA. b XRD pattern of synthesized UiO-66-NH₂

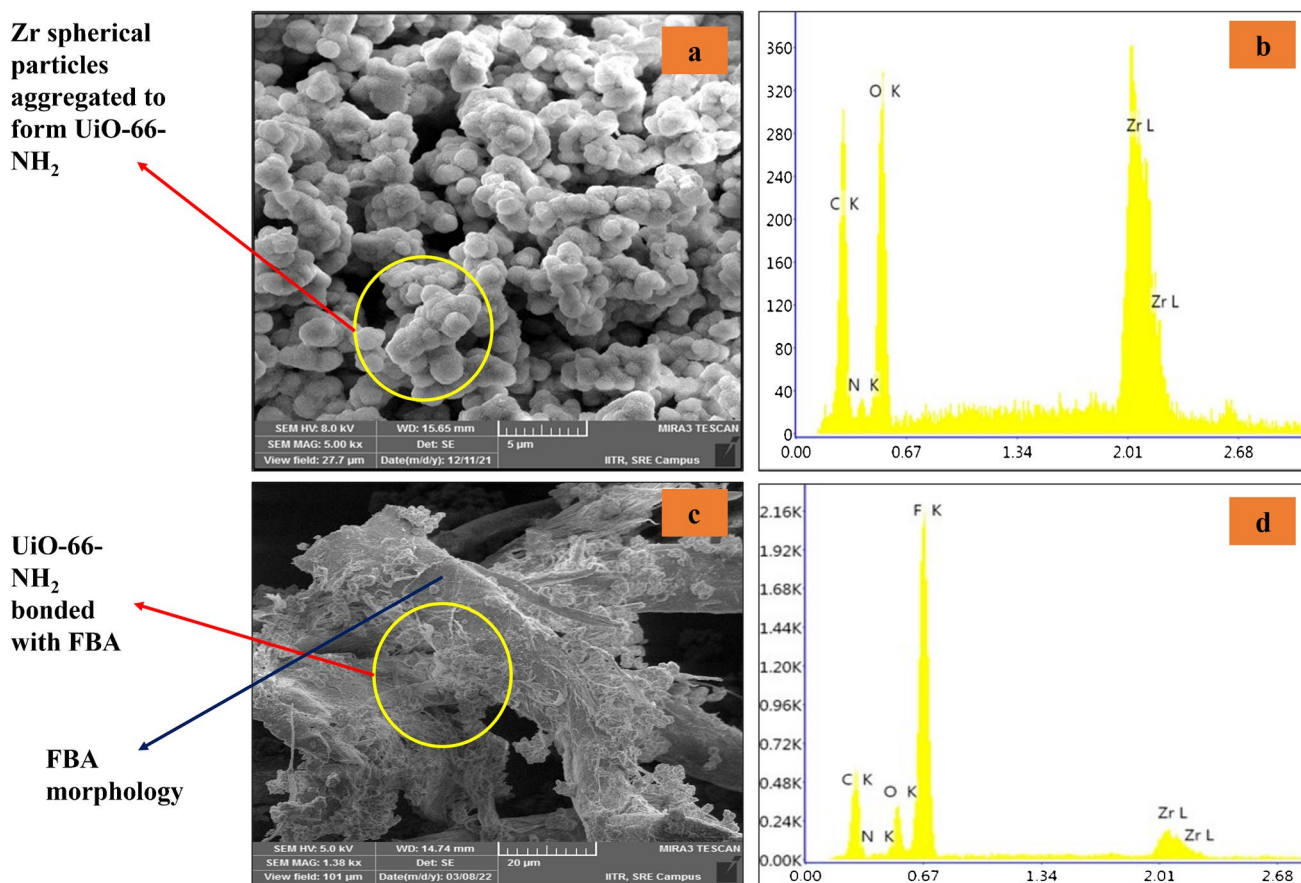


Fig. 2 **a** FESEM image, **b** EDAX pattern of UiO-66-NH₂, **c** FESEM image of UiO-66-NH₂ after interaction with FBA, **d** EDAX pattern of UiO-66-NH₂ after interaction with FBA

and FBAs (Fig. 2d) in which the peak of fluorine atom was observed because fluorine has small size, it can enter into the pores of the MOF and make the bond efficiently.

Before using as sorbent for dSPE, the MOF was activated at 100°C for at least 8 h. The XRD pattern of the MOF after 3 days of storing at room temperature was recorded in which the crystallinity of the MOF was found to be reduced (see Electronic Supplementary Material Fig. S1), but when the MOF was activated at 100°C temperature for at least 6 h, the crystallinity of MOF was regained. In a further study, MOF was activated prior to the analysis.

XPS analysis

The XPS spectra of UiO-66-NH₂ (Fig. 3) indicated the sharp peaks of Zr, C, N, and O, which were further deconvoluted using multipak software. The two peaks of Zr-O bonds correspond to the 3d_{5/2} (180.96 eV) and 3d_{3/2} (183.26 eV) orbitals. The sole peak of nitrogen corresponds to the amino group, having binding energy equal to 401.8 eV, and three deconvoluted peaks in the carbon peak corresponding to COO/C-NH₂ (288.3 eV), C-C/C-H (284.6 eV) bond, and

C-O (286.3 eV) bond, respectively. The oxygen peak was further deconvoluted and shown the two peaks corresponding to Zr-O (530.58 eV) and O=C=O bond (531.47 eV), respectively, as reported in various literatures [38–42].

The XPS spectra of UiO-66-NH₂ (Fig. 4) after interaction with 2-TFM BA were recorded in which the intensity of all elemental peaks was increased, and the new peak of fluorine confirmed the successful interaction of MOF with the FBA. The higher intensity change was observed in the Zr and C peaks as compared to the change, which was a bit lower in the case of O, F, and N, possibly due to the lower concentration of F and hence the interaction. In order to evaluate the formation of new bonds, the peaks of these elements were deconvoluted, and the peaks of N-H-O and N-H-F were obtained in the N, O, and F regions. In the C 1s region, the peaks of the C-F (288.8 eV) bond and Zr-O-C (286.24 eV) were observed that confirmed the successful interaction of UiO-66-NH₂ with this FBA and the bond formation between Zr and carbonyl oxygen which may be a reason for a gradual increase in the intensity of Zr 3d peaks.

The intensity of the carboxylate anion was also increased due to the contribution from 2-TFMBA, which confirms the ionization of FBA at pH 3.20. The N-H-O, Zr-O-C, and

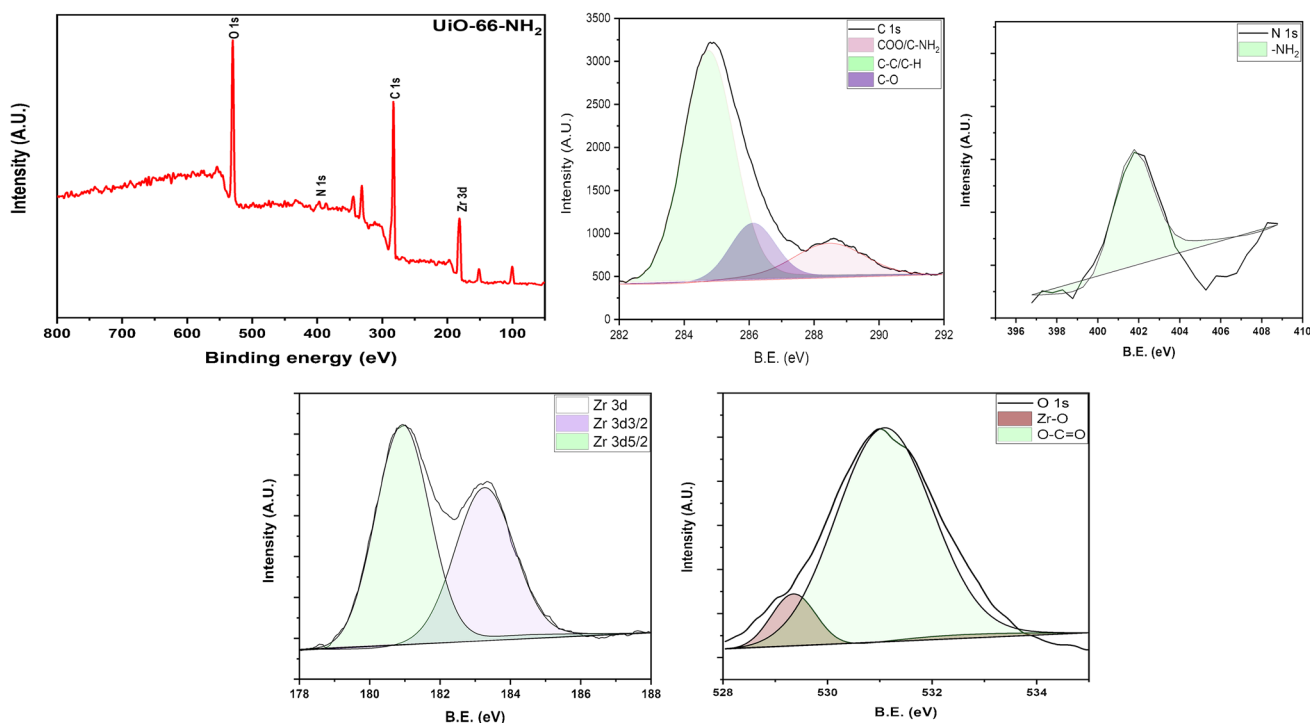


Fig. 3 XPS spectra of UiO-66-NH₂

carboxylate anion peaks can also be observed in the oxygen region at 533.32 eV and 532.77 eV, respectively; the hydrogen bonding is the reason for the increase in the binding energy of NHO bond. The fluorine peak was also deconvoluted and found the specific N–H–F bond, HF, and C–F (due to FBA), which appeared at 685.4 eV, 686.1 eV, and 687.1 eV, respectively [43, 44].

It was also observed that the binding energy of the amino group was shifted positively due to hydrogen bonding with fluorine and shifted negatively in the fluorine region because the electron density of N was shifted to F, as it is a more electronegative atom as compared to N. In another scenario, the binding energy of the amino group was shifted negatively due to charge-assisted hydrogen bonding with O and shifted positively in the O region since the charge density of oxygen transferred to the amino group, as observed by Zhu et al. [45] in the case of fluoride ion. Thus, the NHO and NHF showed peaks at 401.23 eV [46] and 401.8 eV, respectively.

Optimization of the sample preparation method

The method was optimized in terms of elution solvent, elution volume, pH, sorbent weight, adsorption, and desorption time. The effect of these parameters was evaluated by the MS response hence the area of the particular peak. The area

is plotted as the average for each substituted FBA vs. the specified parameter.

Optimization of the elution solvent and elution volume

Different elution solvents like acetonitrile, methanol, dichloromethane, acetonitrile containing 5% of formic acid, and methanol containing 5% of formic acid were used for this study, but ACN containing 5% formic acid was found the optimum elution solvent (Fig. 5a). Further, different amounts of elution solvent ranging from 0.5 to 4.0 ml were tried to get the optimum extraction efficiency (EE) of FBAs, but there was no considerable effect of increasing elution volume on the EE of the FBAs after 3.0 ml of the solvent (Fig. 5b), i.e., ACN containing HCOOH; hence, 3.0 mL of ACN containing 5% HCOOH was chosen in the further study.

Optimization of sorbent weight

To attain the maximum extraction efficiency of FBAs, the different amounts of MOF ranging from 15 to 105 mg were investigated. It was concluded on the basis of GC–MS response that the maximum extraction efficiency was observed in the case of 80 mg UiO-66-NH₂ (Fig. 5c), and there was no significant effect of increasing the amount

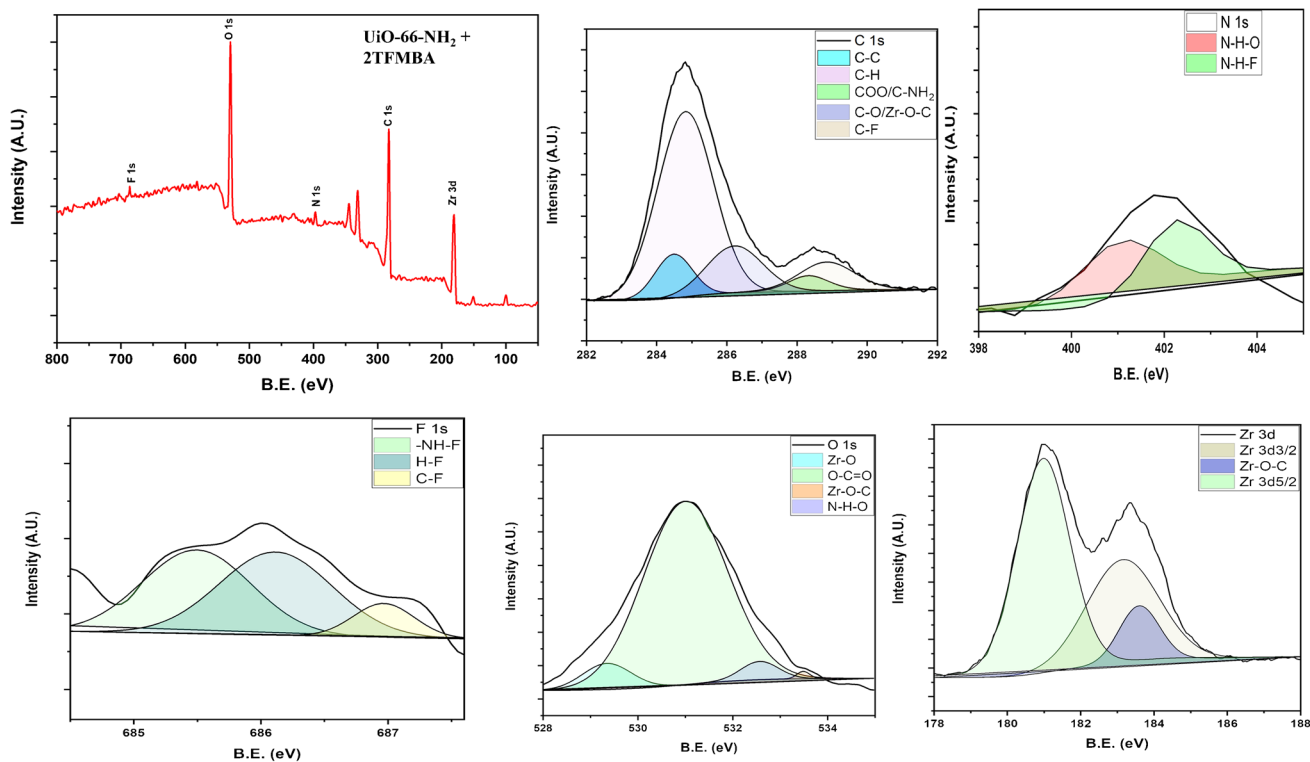


Fig. 4 XPS spectra of UiO-66-NH₂ after interaction with FBA

of MOF on the extraction efficiency of MOF. Therefore, 80 mg UiO-66-NH₂ was selected for further analysis.

pH

It is well-known that the pH of the sample has a significant effect on the surface charge or ionization of the compounds hence on the interaction between functional groups. To get the optimum interaction between the FBAs and UiO-66-NH₂, the response of the different FBAs was recorded in the pH range from 3.00 to 5.90 (Fig. 5d) since the MOF shows high stability in this pH range. The optimum extraction efficiency was obtained in the case of pH 3.20; hence, this value was chosen for further analysis, although there was no additional chemical required for maintaining the pH of the sample because the pH was found to be 3.20 in the case of each FBA after addition of the optimized weight of MOF only.

Stirring vs. ultra-sonification

The different treatments were given to the aqueous solution for obtaining optimum values of extraction efficiency and found that the ultra-sonification was found to be the suitable technique for dispersing the MOF particles to the aqueous solutions and promoting the transfer of FBAs to the surface

of UiO-66-NH₂; hence, the ultra-sonification was chosen for further sample preparation.

Adsorption time

To check the optimum adsorption time, the GC–MS response was recorded at 2–10 min after mixing 80 mg UiO-66-NH₂ with different FBAs at ppb levels. It was observed that there was no significant increase in the area of FBAs as their pentafluorobenzyl esters after 10 min of sonication (Fig. 5e), so the adsorption time of 10 min was used for further study.

Desorption time

Similarly, the desorption time was also optimized, and it was found that there was no significant increase in the GC–MS response after 7 min, so a desorption time of 7 min was used in further experiments (Fig. 5f).

Reusability of the material

The reusability of the material was checked by drying the recovered material at 100°C for 6 h, and found that UiO-66-NH₂ can be reused up to three cycles of adsorption and

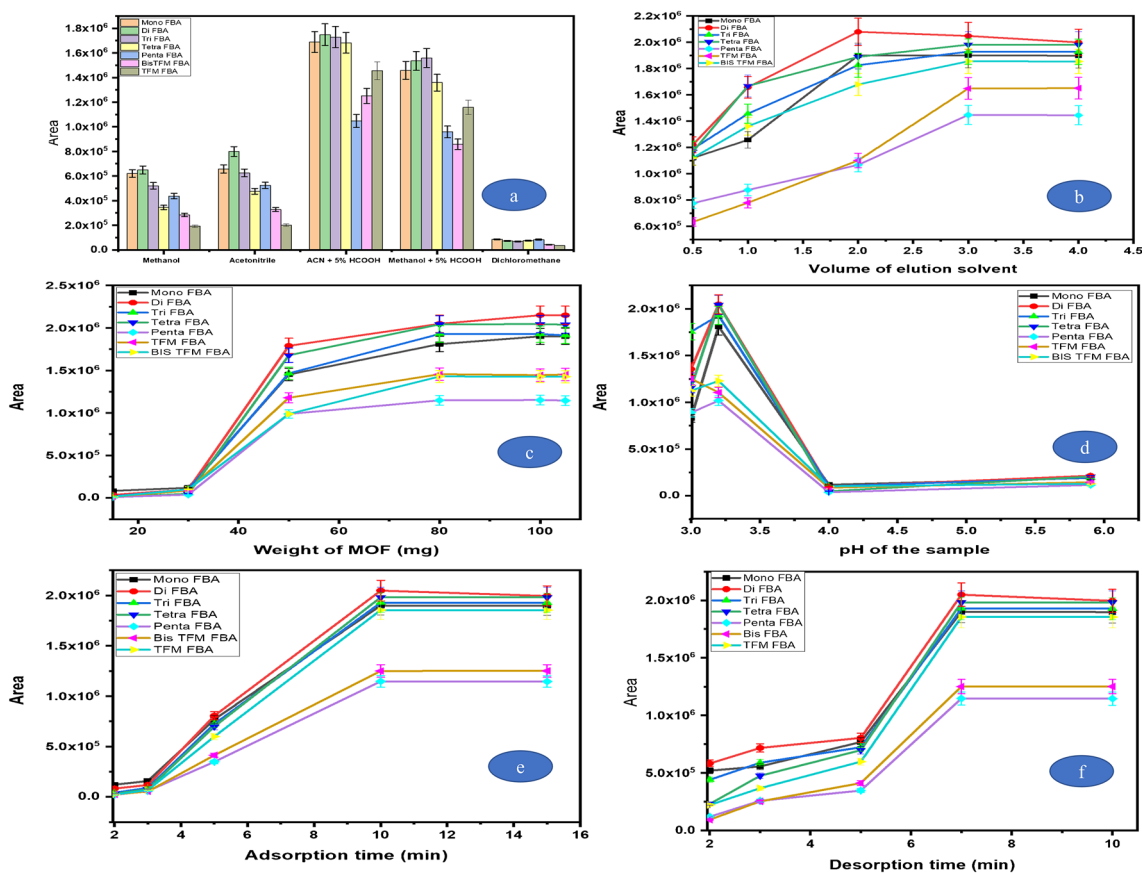


Fig. 5 Optimization of dSPE condition parameters. **a** Recorded area of various FBAs in different elution solvents. **b** Response of various FBAs in different volumes of elution solvent. **c** Response of various FBA after adding different weights. **d** Response of various FBAs at

different pH of the sample. **e** Response of various FBA at different adsorption time. **f** Response of various FBA at different desorption times

desorption; hence, the material is best suited for the extraction of FBAs from aqueous samples. The EE of the third cycle was found to be 96% as compared to the first cycle, in which it was 100% for 2-FBAs, although 67% EE was obtained in the fourth cycle, possibly, due to the saturation of the surface by the salts, which prevents the analyte adsorption on the surface of the MOF or masking of the analyte take place.

Possible mechanism of interaction and molecular sizes of FBAs

The possible mechanism of extraction can be explained on the basis of two types of interactions: first, the hydrogen bonding between the $-NH_2$ group of MOF and the oxygen of the carboxylate group, fluorine atoms of FBAs, and second, the attraction between the Zr and oxygen of the carbonyl group (HSAB principle) of the FBAs. When the acid containing eluted was added, the hydrogen bonding was destroyed, and the FBAs were eluted as a result. The phenomenon was confirmed by IR spectra and FESEM image, EDAX pattern, and the fact that the FBAs ionized at

pH 3.20, so the COOH group was dissociated, and charge-assisted hydrogen bonding took place as shown in Fig. 6b. The molecular size of each FBA was estimated using Multiwfn software [47] and found that the FBAs size lies in range from 6.15 to 7.54 Å (Fig. 6a) which is lesser than the pore window of UiO-66-NH₂. Thus, the FBAs present in the sample can enter to the pores of the MOF and be adsorbed via hydrogen bonding and other interactions as described by Mao et al. [48].

Validation of the method and its comparison

The method was validated in terms of linearity, specificity, system precision, and repeatability. The samples of Milli-Q, seawater, and tap water were spiked with the known concentration of FBAs, and the procedure was repeated according to the “Dispersive SPE and derivatization procedure” section. The extraction efficiency for the FBAs was found in the range from 98.45–104.39% for Milli-Q water samples, 69.13–105.48% for salt-rich seawater samples, and 92.56–103.50% for tap water samples (Table 2) with the

maximum RSD value up to 6.87%. In terms of specificity, there were no interfering peaks in the chromatogram that may affect the quantitative analysis of FBAs, but multiple peaks can be generated due to the hydrolysis or decomposition of the derivatizing agent PFBBr so it should be stored in the tight container or under inert gas. The linear response of the detector in the case of each FBA was recorded, and a good value of regression greater than 0.98 was obtained, as

$$\% \text{ Extraction efficiency} = \frac{\text{measured concentration of FBA in sample solution} - \text{concentration of FBA in blank solution}}{\text{Added concentration of FBA}} * 100$$

The method was also compared with the existing method reported in the literature for the determination of FBAs in water samples (Table 3). The literature showed that the SPE could offer a higher enrichment in the concentration, but the process uses a large volume of high-purity hazardous solvents. Also, the automated SPE is nowadays very expensive instrument, and the cartridges used in the SPE are also single-use, so this method overcomes these advantages. Although the conventional SPE offers a bit higher enrichment factor as compared to this method, but this method can be used for cost-effective routine analysis of the FBAs at ng/mL level in the aqueous samples.

shown in Table 1. The LOD and LOQ value was determined on the basis of signal-to-noise ratio (S/N), which was taken at least 3.0 for LOD and 10.0 for LOQ. The enrichment factor was taken as 28.57 in this study since 20 mL of the sample was taken for the extraction, and finally, it was collected in 0.700 mL acetonitrile.

The extraction efficiency (EE) was calculated using the following formulae and provided in Table 2:

Applications

Since the material has very useful applications in various water matrices like reservoir water, leaching studies, and hydrogeological studies and these matrices have different characteristics, the applications of the synthesized material were determined in artificial seawater and tap water. The artificial seawater solution was prepared according to ASTM D1141-98 with the salt compositions given in Table S2 (see Electronic Supplementary Material Table S2). The tap water was collected from the campus. All the water samples except the Milli-Q water sample were filtered through a 0.45- μm membrane filter

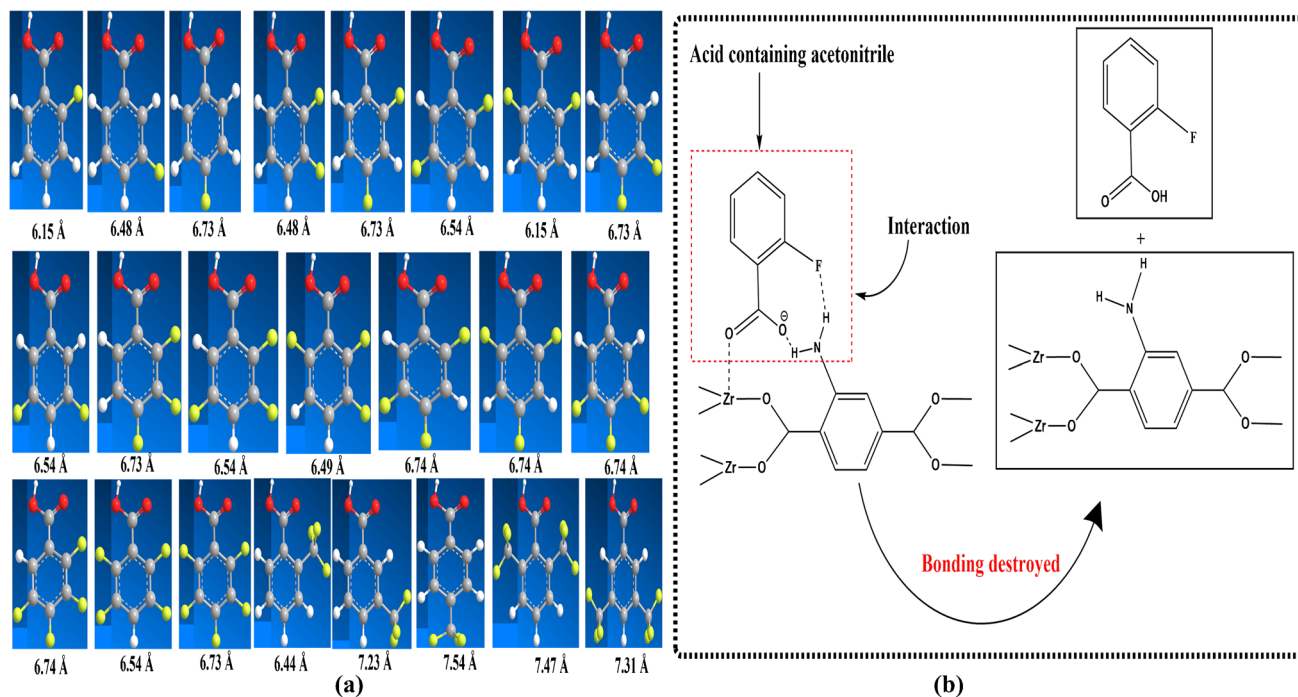


Fig. 6 **a** Calculated molecular size of different FBAs, **b** interaction mechanism of UiO-66-NH₂ with FBA

Table 1 Linearity, retention time (RT), LOD, and LOQ data for all FBAs

Compound name	Linearity equation	R^2	LOD (ng/mL)	RT	LOQ (ng/mL)	Precision (% RSD, $n=3$)	
						Intra-day	Inter-day
2-Fluorobenzoic acid	$Y=35708.3X+48449.7$	0.9844	0.37	13.05	1.23	2.68	4.12
3-Fluorobenzoic acid	$Y=295426X+3245241$	0.9978	0.40	12.31	1.33	3.32	6.21
4-Fluorobenzoic acid	$Y=163118X+263000$	0.9918	0.40	12.37	1.33	2.47	3.98
2,3-Difluorobenzoic acid	$Y=297801X+567436$	0.9971	0.50	12.89	1.67	1.89	4.02
2,4-Difluorobenzoic acid	$Y=36823.5X+116142$	0.9969	0.67	12.20	2.27	2.16	4.85
2,5-Difluorobenzoic acid	$Y=174358X+1119220$	0.9813	0.40	12.38	1.33	2.72	4.96
2,6-Difluorobenzoic acid	$Y=55036.9X+330155$	0.9848	0.40	12.52	1.37	1.25	2.86
3,4-Difluorobenzoic acid	$Y=60000X+249960$	0.9969	0.40	12.13	1.37	2.98	3.77
3,5-Difluorobenzoic acid	$Y=468147X+196001$	0.9840	0.53	11.30	1.77	2.75	3.33
2,3,4-Trifluorobenzoic acid	$Y=9382.06X+30792.7$	0.9944	0.83	12.20	2.77	2.14	4.25
2,3,5-Trifluorobenzoic acid	$Y=119315X+151872$	0.9957	0.80	11.53	2.67	1.12	3.69
2,4,5-Trifluorobenzoic acid	$Y=19169.5X+432760$	0.9939	0.33	11.64	1.17	2.32	4.22
2,3,6-Trifluorobenzoic acid	$Y=255302X+240116$	0.9855	0.87	12.03	2.87	1.21	2.47
2,4,6-Trifluorobenzoic acid	$Y=61489.5X+84660.1$	0.9857	1.07	11.20	3.53	2.30	4.69
3,4,5-Trifluorobenzoic acid	$Y=98622.1X+168255$	0.9938	1.03	11.25	3.43	0.92	1.99
2,3,4,5-Tetrafluorobenzoic acid	$Y=103947X+162585$	0.9847	1.10	11.39	3.27	2.75	5.12
2,3,5,6-Tetrafluorobenzoic acid	$Y=100147X+204284$	0.9976	1.17	11.28	3.33	2.98	5.98
2,3,4,5,6-Pentafluorobenzoic acid	$Y=1219.15X+8123.07$	0.9986	0.83	10.60	2.67	3.45	6.21
2-(Trifluoromethyl)-benzoic acid	$Y=88,988.3X+140,729$	0.9935	0.37	12.66	1.13	1.15	2.56
3-(Trifluoromethyl)-benzoic acid	$Y=86296.9X+365982$	0.9949	0.47	12.10	1.57	1.36	2.86
4-(Trifluoromethyl)-benzoic acid	$Y=60716.7X+332944$	0.9930	0.53	12.31	1.77	1.48	3.02
2,6-Bis(trifluoromethyl)benzoic acid	$Y=52038.6X+36338.8$	0.9995	0.93	9.97	3.00	2.67	4.65
3,5-Bis(trifluoromethyl)benzoic acid	$Y=29879.5X+165625$	0.9844	0.93	11.40	3.00	2.37	4.44

and spiked at the known concentration of FBAs. Thereafter, the procedure defined in the “**Dispersive SPE and derivatization procedure**” section was followed.

The chromatograms of each FBA extracted from tap water are represented in Fig. 7.

Batch-to-batch reproducibility of the UiO-66-NH₂

Since the synthesized material is synthesized for its frequent use in routine analysis, its batch-to-batch reproducibility was determined for 3 different batches. The BET data of synthesized batches are presented in Table S3 (see Electronic Supplementary Material Table S3).

Conclusion

In this study, we reported a synthesized MOF as an adsorbent of dSPE for the enrichment and extraction of FBAs from Milli-Q, tap water, and seawater samples. The described method showed a lower detection limit and good extraction efficiency for the determination of trace levels of FBAs in water samples. As a result, tri-substituted FBA, some of the mono, di-FBA, and Bis-TFM substituted FBA are recommended for use in the high salinity water samples. The proposed method is simple, rapid, and inexpensive; hence, this study not only provided a sensitive method for the determination of FBAs from water samples but also demonstrated the practicality of UiO-66-NH₂ MOF material as adsorption in

Table 2 Extraction efficiency of the 23 FBAs in Milli-Q, seawater, and tap water (*n* = 3)

Compound name	Added concentration (ng/mL)	EE% (Milli-Q water) (%EE ± %RSD)	EE% (sea water) (%EE ± %RSD)	EE% (tap water) (%EE ± %RSD)
2-Fluorobenzoic acid	6.9	103.07 ± 0.10	102.47 ± 4.70	99.05 ± 3.44
3-Fluorobenzoic acid	7.7	100.89 ± 6.43	79.57 ± 2.43	100.14 ± 1.66
4-Fluorobenzoic acid	7.1	102.60 ± 3.46	87.56 ± 4.98	103.50 ± 2.81
2,3-Difluorobenzoic acid	11.1	103.48 ± 3.10	74.70 ± 1.99	96.88 ± 1.10
2,4-Difluorobenzoic acid	11.2	103.11 ± 1.44	76.70 ± 1.78	99.88 ± 1.22
2,5-Difluorobenzoic acid	11.7	103.21 ± 5.03	74.87 ± 1.79	102.91 ± 2.24
2,6-Difluorobenzoic acid	9.8	98.45 ± 1.32	70.62 ± 0.19	95.50 ± 3.84
3,4-Difluorobenzoic acid	14.3	102.90 ± 6.05	73.38 ± 1.67	101.07 ± 3.61
3,5-Difluorobenzoic acid	12.3	102.28 ± 2.34	71.39 ± 2.28	99.59 ± 2.87
2,3,4-Trifluorobenzoic acid	10.5	103.78 ± 2.06	100.17 ± 0.94	99.10 ± 2.45
2,3,5-Trifluorobenzoic acid	8.6	102.55 ± 1.08	100.71 ± 4.39	99.71 ± 3.00
2,4,5-Trifluorobenzoic acid	9.9	104.39 ± 1.84	100.46 ± 3.85	94.67 ± 2.42
2,3,6-Trifluorobenzoic acid	6.9	102.88 ± 2.89	94.46 ± 4.85	98.74 ± 2.56
2,4,6-Trifluorobenzoic acid	9.1	103.33 ± 1.88	105.48 ± 3.10	102.17 ± 1.82
3,4,5-Trifluorobenzoic acid	8.8	100.93 ± 3.54	101.57 ± 0.70	100.99 ± 2.53
2,3,4,5-Tetrafluorobenzoic acid	7.6	103.70 ± 4.87	75.28 ± 2.45	98.11 ± 3.12
2,3,5,6-Tetrafluorobenzoic acid	7.5	104.19 ± 6.36	69.13 ± 3.22	100.46 ± 0.12
2,3,4,5,6-Pentafluorobenzoic acid	9.2	99.72 ± 6.87	87.96 ± 0.92	92.56 ± 1.45
2-(Trifluoromethyl)-benzoic acid	8.2	103.21 ± 5.82	74.25 ± 2.75	102.24 ± 1.67
3-(Trifluoromethyl)-benzoic acid	8.3	103.20 ± 2.37	77.13 ± 4.40	100.44 ± 0.81
4-(Trifluoromethyl)-benzoic acid	7.3	102.97 ± 2.92	74.02 ± 2.17	103.10 ± 2.20
2,6-Bis(trifluoromethyl)benzoic acid	10.4	102.15 ± 1.34	97.79 ± 0.63	98.95 ± 3.01
3,5-Bis(trifluoromethyl)benzoic acid	8.7	103.07 ± 4.35	103.84 ± 3.74	99.20 ± 2.45

Table 3 Comparison of the described method with the literature reported GC-based methods

Sample	Extraction technique	No. of analytes	Sample volume required(mL)	Determination technique & derivatization time	IDL (ng/mL)	Enrichment factor	% RSD	Sorbent weight (mg) and type	Reference
Reservoir water	SPE	15	250	GC-MS NICI (30 min)	10-60	500	0.14-0.28 (4-FBA)	200 mg, disposable	[21]
Reservoir water	SPE	16	250	GC-MS EI (immediately) but used derivatizing agent is discontinued	0.1	833.33	0.03-0.05	200 mg, disposable	[25]
Tap water and reservoir water	SPE	21	100	GC-MS EI (24 h)	1.9-12.1	250	< 12.6	225 mg, disposable	[23]
Ground and reservoir water	SPE	06	100	GC-MS EI (24 h)	1.9-9.6	250	< 14.5	225 mg, disposable	[27]
Milli-Q water, tap water, and artificial seawater	dSPE	23	20	GC-MS NICI (30 min)	0.33-1.17	28.57	< 6.86	80 mg, reusable	This work

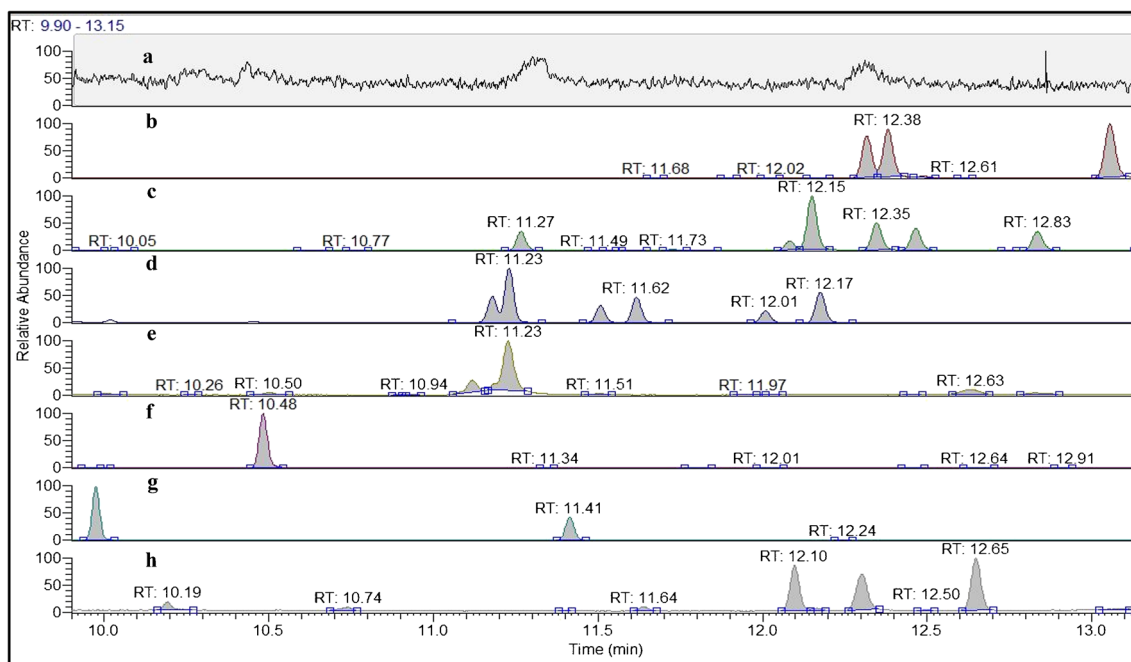


Fig. 7 Chromatograms of **a** blank tap water without spiking FBA, **b** tap water containing mono-FBAs, **c** tap water containing Di-FBAs, **d** tap water containing Tri-FBAs, **e** tap water containing tetra-FBAs,

f tap water containing penta-FBA, **g** tap water containing Bis-TFM-FBAs, **h** tap water containing TFM-FBAs at their SIM ions

solid-phase extraction techniques to extract FBAs from salt-rich water samples. In another way, the single-use materials can be displaced by the synthesized MOF, and the simple dSPE can be used in the routine analysis in place of the expensive automated SPE technique.

Supplementary Information The online version contains supplementary material available at <https://doi.org/10.1007/s00216-023-04728-1>.

Acknowledgements The authors are very thankful to the Ministry of Education, Government of India, for providing the Prime Minister Research Fellowship, and the Indian Institute of Technology Roorkee, Roorkee, India, for providing the characterization facilities and other support.

Funding This work is financially supported by the Ministry of Education, Government of India, and the Institute of Technology Roorkee, Roorkee, India (Grant no. PM-31–22-681–414).

Declarations

Ethics approval Not applicable.

Source of biological material Not applicable.

Statement on animal welfare Not applicable.

Conflict of interest The authors declare no competing interests.

References

1. Khatibi SA, Hamidi S, Siahi-Shadbad MR. Current trends in sample preparation by solid-phase extraction techniques for the determination of antibiotic residues in foodstuffs: a review. *Crit Rev Food Sci Nutr.* 2021;61:3361–82.
2. Augusto F, Hantao LW, Mogollón NGS, Braga SCGN. New materials and trends in sorbents for solid-phase extraction. *TrAC - Trends Anal Chem.* 2013;43:14–23.
3. Hamidi S, Taghvi A, Mazouchi N. Micro solid phase extraction using novel adsorbents. *Crit Rev Anal Chem.* 2021;51:103–14.
4. He YP, Tan YX, Wang F, Zhang J. Microporous zinc tris[(4-carboxyl)phenylduryl]amine framework with an unusual topological net for gas storage and separation. *Inorg Chem.* 2012;51:1995–7.
5. Murray LJ, Dinc M, Long JR. Hydrogen storage in metal-organic frameworks. *Chem Soc Rev.* 2009;38:1294–314.
6. Sculley J, Yuan D, Zhou HC. The current status of hydrogen storage in metal-organic frameworks - Updated. *Energy Environ Sci.* 2011;4:2721–35.
7. Piscopo CG, Trapani F, Polyzoidis A, Schwarzer M, Pace A, Loebbecke S. Positive effect of the fluorine moiety on the oxygen storage capacity of UiO-66 metal-organic frameworks. *New J Chem.* 2016;40:8220–4.
8. Abid HR, Pham GH, Ang H, Tade MO, Wang S. Journal of Colloid and Interface Science Adsorption of CH₄ and CO₂ on Zr-metal organic frameworks. *J Colloid Interface Sci.* 2012;366:120–4.
9. Chowdhury P, Bikkina C, Gumma S. Gas adsorption properties of the chromium-based metal organic framework MIL-101. *J Phys Chem C.* 2009;113:6616–21.

10. Lee J, Farha OK, Roberts J, Scheidt KA, Nguyen ST, Hupp JT. Metal-organic framework materials as catalysts. *Chem Soc Rev*. 2009;38:1450–9.
11. Du PY, Gu W, Liu X. A three-dimensional Nd(III)-based metal-organic framework as a smart drug carrier. *New J Chem*. 2016;40:9017–20.
12. Ge D, Peng J, Qu G, Geng H, Deng Y, Wu J, Cao X, Zheng J, Gu H. Nanostructured Co(II)-based MOFs as promising anodes for advanced lithium storage. *New J Chem*. 2016;40:9238–44.
13. Gholipour-Ranjbar H, Soleimani M, Naderi HR. Application of Ni/Co-based metal-organic frameworks (MOFs) as an advanced electrode material for supercapacitors. *New J Chem*. 2016;40:9187–93.
14. Hu H, Lou X, Li C, Hu X, Li T, Chen Q, Shen M, Hu B. A thermally activated manganese 1,4-benzenedicarboxylate metal organic framework with high anodic capability for Li-ion batteries. *New J Chem*. 2016;40:9746–52.
15. Kandiah M, Nilsen MH, Usseglio S, Jakobsen S, Olsbye U, Tilset M, Larabi C, Quadrelli EA, Bonino F, Lillerud KP. Synthesis and stability of tagged UiO-66 Zr-MOFs. *Chem Mater*. 2010;22:6632–40.
16. Xia L, Liu L, Xu X, Zhu F, Wang X, Zhang K, Yang X, You J. Determination of chlorophenoxy acid herbicides by using a zirconium-based metal-organic framework as special sorbent for dispersive micro-solid-phase extraction and high-performance liquid chromatography. *New J Chem*. 2017;41:2241–8.
17. Fei H, Shin J, Meng YS, Adelhardt M, Sutter J, Meyer K, Cohen SM. Reusable oxidation catalysis using metal-monocatecholato species in a robust metal-organic framework. *J Am Chem Soc*. 2014;136:4965–73.
18. Siu PW, Brown ZJ, Farha OK, Hupp JT, Scheidt KA. A mixed dicarboxylate strut approach to enhancing catalytic activity of a de novo urea derivative of metal-organic framework UiO-67. *Chem Commun*. 2013;49:10920–2.
19. Lichtenberger GJ. Field applications of interwell tracers for reservoir characterization of enhanced oil recovery pilot area. Paper SPE 21652 presented at the Production Operations Symposium. Oklahoma City, OK; 1991. <https://doi.org/10.2523/21652-MS>
20. Kumar A, Sharma C. Advances in the analytical methods for the determination of fluorinated aromatic carboxylic acids in aqueous matrices: a review. *J Sep Sci*. 2022;45:78–93.
21. Galdiga CU, Greibrokk T. Ultra trace determination of fluorinated aromatic carboxylic acids in aqueous reservoir fluids by solid phase extraction in combination with negative ion chemical ionisation mass spectrometry after derivatisation with pentafluorobenzyl bromide. *Fresenius J Anal Chem*. 1998;361:797–802.
22. Kubica P, Garraud H, Szpunar J, Lobinski R. Sensitive simultaneous determination of 19 fluorobenzoic acids in saline waters by solid-phase extraction and liquid chromatography-tandem mass spectrometry. *J Chromatogr A*. 2015;1417:30–40.
23. Müller K, Seubert A. Ultra trace determination of fluorobenzoic acids in tap and reservoir water using solid-phase extraction and gas chromatography-mass spectrometry. *J Chromatogr A*. 2012. <https://doi.org/10.1016/j.chroma.2012.08.050>.
24. Gavrilenko MA, Gavrilenko NA. Solid-phase extraction of fluorinated benzoic acids for the chromatographic analysis of oil tracer agents. *Mendeleev Commun*. 2015;25:159–60.
25. Galdiga CU, Greibrokk T. Ultra-trace determination of fluorinated aromatic carboxylic acids in aqueous reservoir fluids using solid-phase extraction in combination with gas chromatography-mass spectrometry. *J Chromatogr A*. 1998;793:297–306.
26. Müller K, Seubert A. Separation and determination of fluorobenzoic acids using ion chromatography-electrospray mass spectrometry. *J Chromatogr A*. 2012;1270:96–103.
27. Müller K, Seubert A. Ultra trace determination of fluorobenzoic acids in reservoir and ground water using isotope dilution gas chromatography mass spectrometry. *Isotopes Environ Health Stud*. 2014;50:277–84.
28. Kvernheim AL. Produced water-composition and analysis. ENS '97: 4 environment Northern Seas conference, Norway; 1998. https://inis.iaea.org/search/search.aspx?orig_q=RN:30018811
29. Essam Abdul-Jalil Saeed, Hamed H, Ayad A. Components and treatments of oilfield produced water. *Al-Khawarizmi Eng J*. 2010;(6):24–30.
30. Igundu ET, Chen GZ. Produced water treatment technologies. *Int J Low-Carbon Technol*. 2014;9:157–77.
31. Bader MSH. Seawater versus produced water in oil-fields water injection operations. *Desalination*. 2007;208:159–68.
32. Vermoordele F, Vimont A, Serre C, De Vos D. An amino-modified Zr-terephthalate metal-organic framework as an acid-base catalyst for cross-aldol condensation. *Chem Commun*. 2011;47:1521–3.
33. Luu CL, Van Nguyen TT, Nguyen T, Hoang TC. Synthesis, characterization and adsorption ability of UiO-66-NH₂. *Adv Nat Sci Nanosci Nanotechnol*. 2015;6(2).
34. Kumar A, Sharma C. Recent update of the various sources originating ghost peaks in gas chromatography: a review. *J Chromatogr A*. 2022;1685: 463625.
35. Zhang X, Zhang Y, Wang T, Fan Z, Zhang G. A thin film nanocomposite membrane with pre-immobilized UiO-66-NH₂ toward enhanced nanofiltration performance. *RSC Adv*. 2019;9:24802–10.
36. Dalapati R, Zang L. Aqueous medium fluoride anion sensing by fluorophore encapsulated UiO-66 type zirconium metal-organic framework. *Chemistry Proceedings*. 2021;5.
37. Rundle RE, Nakamoto Kazuo, Margoshes M. Stretching frequencies as a function of distances in hydrogen bonds. *J Am Chem Soc*. 1955;77:6480–6.
38. Zhang N, Li D, Mu M, Lu M. Partially fluorinated UiO-66-NH₂(Zr): positive effect of the fluorine moiety on the adsorption capacity for environmental pollutants of metal-organic frameworks. *Chem Eng J*. 2022;448: 137467.
39. Tian P, He X, Li W. Zr-MOFs based on Keggin-type polyoxometalates for photocatalytic hydrogen production. *J Mater Sci*. 2018;53:12016–29.
40. Wang Y, Li L, Dai P, Yan L, Cao L, Gu X, Zhao X. Missing-node directed synthesis of hierarchical pores on a zirconium metal-organic framework with tunable porosity and enhanced surface acidity: via a microdroplet flow reaction. *J Mater Chem A*. 2017;5:22372–9.
41. Teeparthi SR, Awin EW, Kumar R. Dominating role of crystal structure over defect chemistry in black and white zirconia on visible light photocatalytic activity. *Sci Rep*. 2018;8:1–12.
42. Ibrahim AH, El-Mehalmey WA, Haikal RR, Safy MEA, Amin M, Shatla HR, Karakalos SG, Alkordi MH. Tuning the chemical environment within the UiO-66-NH₂ nanocages for charge-dependent contaminant uptake and selectivity. *Inorg Chem*. 2019. <https://doi.org/10.1021/acs.inorgchem.9b01611>.
43. Saito Y. Adsorption of anhydrous hydrogen fluoride onto silicon and native oxide by XPS. *Surf Sci Spectra*. 1999;6:228–36.
44. Kealey CP, Klapötke TM, McComb DW, Robertson MI, Winfield JM. Fluorination of polycrystalline diamond films and powders. An investigation using FTIR spectroscopy, SEM, energy-filtered TEM, XPS and fluorine-18 radiotracer methods. *J Mater Chem*. 2001;11:879–86.
45. Zhu H, Huang J, Zhou Q, Lv Z, Li C, Hu G. Enhanced luminescence of NH₂-UiO-66 for selectively sensing fluoride anion in water medium. *J Lumin*. 2019;208:67–74.
46. Tanaka Y, Matsuo Y, Komiya T, Tsutsumi Y, Doi H, Yoneyama T, Hanawa T. Characterization of the spatial immobilization manner of poly(ethylene glycol) to a titanium surface with immersion and

- electrodeposition and its effects on platelet adhesion. *J Biomed Mater Res Part A*. 2010;92:350–8.
47. Lu T, Chen F. Multiwfn: a multifunctional wavefunction analyzer. *J Comput Chem*. 2012;33:580–92.
 48. Mao X, Xiao W, Wan Y, Li Z, Luo D, Yang H. Dispersive solid-phase extraction using microporous metal-organic framework UiO-66: Improving the matrix compounds removal for assaying pesticide residues in organic and conventional vegetables. *Food Chem*. 2021;345: 128807.

Publisher's note Springer Nature remains neutral with regard to jurisdictional claims in published maps and institutional affiliations.

Springer Nature or its licensor (e.g. a society or other partner) holds exclusive rights to this article under a publishing agreement with the author(s) or other rightsholder(s); author self-archiving of the accepted manuscript version of this article is solely governed by the terms of such publishing agreement and applicable law.